

Concentration Dependent Sedimentation of Colloidal Rods

Z. Dogic*, A.P. Philipse†, S. Fraden*, J.K.G. Dhont† ‡ *

*Complex Fluid Group, Department of Physics, Brandeis University, Waltham MA 02454,

†van't Hoff Laboratory, Utrecht University, Padualaan8, 3584 CH Utrecht, The Netherlands, ‡Forschungszentrum Jülich, IFF, Weiche Materie, 52425 Jülich, Germany

(October 31, 2018)

In the first part of this paper, an approximate theory is developed for the leading order concentration dependence of the sedimentation coefficient for rod-like colloids/polymers/macromolecules. To first order in volume fraction φ of rods, the sedimentation coefficient is written as $1 + \alpha\varphi$. For large aspect ratio L/D (L is the rod length, D its thickness) α is found to very like $\propto (\frac{L}{D})^2 / \log(\frac{L}{D})$. This theoretical prediction is compared to experimental results. In the second part, experiments on *fd*-virus are described, both in the isotropic and nematic phase. First order in concentration results for this very long and thin (semi-flexible) rod are in agreement with the above theoretical prediction. Sedimentation profiles for the nematic phase show two sedimentation fronts. This result indicates that the nematic phase becomes unstable with the respect to isotropic phase during sedimentation.

I. INTRODUCTION

There is extensive literature concerned with sedimentation behaviour of spherically shaped colloidal particles (for a review see ref. [1]). Essentially exact predictions can be made for the sedimentation velocity of spherical colloids to first order in concentration [2]. For non-spherical colloids a similar exact prediction is non-existent. The only attempt to calculate the first order concentration dependence of the sedimentation velocity for rod like colloids we are aware of is due to Peterson [3]. This theory is based on approximate, orientationally pre-averaged hydrodynamic interactions between the colloidal rods and a rather crude estimate of certain multiple integrals that represent the ensemble averaged velocity. As yet there are no accurate expressions for hydrodynamic interaction tensors for rods. In the first part of the present paper, in section II, we calculate these interaction tensors in a mean-field approximation. In section III we use this approximate expression for the hydrodynamic interaction functions to derive an explicit expression for the first order in concentration coefficient of the sedimentation velocity as a function of the aspect ratio of the rods. This expression is found to agree remarkably well with Peterson's result for aspect ratios less than about 30. For larger aspect ratios our result for the first order in concentration coefficient is much larger then Peterson's prediction. In the second part of this paper, section IV, sedimentation experiments on *fd*-virus are discussed. Experiments are done at low concentration to find the first order concentration dependence, which is compared to the theory mentioned above. In addition, sedimentation experiments at larger concentrations, including the nematic phase are performed.

II. HYDRODYNAMIC INTERACTION BETWEEN LONG AND THIN RODS

In order to calculate sedimentation velocities, the connection between translational and angular velocities, and hydrodynamic forces and torques must be found. In the present section such a relation will be established for two rods on the Rodne-Prager level, that is, with the neglect of reflection contributions between the rods. Considering only two rods limits the discussion on the sedimentation velocity to first order in concentration. Reflection contributions to the two-rod hydrodynamic interaction functions and multi-body rod interactions are both probably small in comparison to the Rodne-Prager terms, due to the fact that the distance between segments of different rods is of the order of the length of the rods, at least in the isotropic state. A Rodne-Prager approximation could therefore work quite well for long and thin rods, although explicit results for reflection contributions should be obtained to confirm this intuition.

For the low Reynolds numbers under consideration, the translational velocities \mathbf{v}_j , $j = 1, 2$, and the angular velocities $\mathbf{\Omega}_j$ are linearly related to the hydrodynamic forces \mathbf{F}_j^h and torques \mathbf{T}_j^h that the fluid exerts on the rods,

$$\begin{pmatrix} \mathbf{v}_1 \\ \mathbf{v}_2 \\ \mathbf{\Omega}_1 \\ \mathbf{\Omega}_2 \end{pmatrix} = - \begin{pmatrix} M_{11}^{TT} & M_{12}^{TT} & M_{11}^{TR} & M_{12}^{TR} \\ M_{21}^{TT} & M_{22}^{TT} & M_{21}^{TR} & M_{22}^{TR} \\ M_{11}^{RT} & M_{12}^{RT} & M_{11}^{RR} & M_{12}^{RR} \\ M_{21}^{RT} & M_{22}^{RT} & M_{21}^{RR} & M_{22}^{RR} \end{pmatrix} \cdot \begin{pmatrix} \mathbf{F}_1^h \\ \mathbf{F}_2^h \\ \mathbf{T}_1^h \\ \mathbf{T}_2^h \end{pmatrix}. \quad (1)$$

The superscripts “T” and “R” refer to translation and rotation, respectively, while the superscript “h” on the forces and torques refer to their hydrodynamic origin. On the Brownian time scale, the 3×3 -dimensional mobility matrices \mathbf{M} are functions of the positions of the centers of the two rods and their orientation.

As will turn out, in order to find the sedimentation velocity, we need expressions for $\mathbf{M}_{\mathbf{I}\mathbf{J}}^{\mathbf{T}\mathbf{T}}$, for which approximations are obtained in subsection II B. As a first step, the fluid flow field generated by a translating rod must be calculated. This is the subject of subsection II A. Rotation of rods also plays a role in sedimentation, but as will turn out, to first order in concentration and with the neglect of hydrodynamic reflection contributions, these do not contribute to the sedimentation velocity. Explicit expressions pertaining to the hydrodynamics of rotating rods are derived in the same spirit as for translating rods in appendix A. Subsection II C contains some concluding remarks.

For the hydrodynamic calculations the rods will be thought of as a rigid string of spherical beads with diameter D . The length of the rods is L , and there are $n + 1 = L/D$ beads per rod, with n an even integer.

A. Flow field generated by a translating rod

The flow field generated by a rod that consists of $n + 1$ beads is given by,

$$\mathbf{u}(\mathbf{r}) = \sum_{j=-n/2}^{n/2} \oint_{\partial V_j} dS' \mathbf{T}(\mathbf{r} - \mathbf{r}') \cdot \mathbf{f}_j(\mathbf{r}'), \quad (2)$$

where \mathbf{T} is the Oseen tensor,

$$\mathbf{T}(\mathbf{r}) = \frac{1}{8\pi\eta_0 r} \left[\hat{\mathbf{I}} + \hat{\mathbf{r}}\hat{\mathbf{r}} \right], \quad (3)$$

with η_0 the shear viscosity of the solvent and $\hat{\mathbf{r}} = \mathbf{r}/r$ the unit position vector. Furthermore, $\mathbf{f}_j(\mathbf{r}')$ is the force per unit area that a surface element at \mathbf{r}' of bead j exerts on the fluid, and ∂V_j is the spherical surface of bead j . For long and thin rods, the distances \mathbf{r} of interest, relative to the positions of the beads, are those for which $r \gg D$, with D the diameter of the beads. Now write $\mathbf{r}' = \mathbf{r}_j + \mathbf{R}'$ with \mathbf{r}_j the position coordinate of the j^{th} bead, so that $R' = D/2$, and Taylor expand the Oseen tensor in eq.(2) with respect to \mathbf{R}' . Keeping only the first term in this Taylor expansion leads to relative errors of the order $R'/r \sim D/L$. Up to that order we then find,

$$\mathbf{u}(\mathbf{r}) = - \sum_{j=-n/2}^{n/2} \mathbf{T}(\mathbf{r} - \mathbf{r}_j) \cdot \mathbf{F}_j^h, \quad (4)$$

with,

$$\mathbf{F}_j^h = - \oint dS' \mathbf{f}_j(\mathbf{r}'), \quad (5)$$

the total force that the fluid exerts on bead j . With the neglect of end-effects this force is equal for each bead, $\mathbf{F}_j \equiv \mathbf{F}^h/(n + 1) = \frac{D}{L}\mathbf{F}^h$, with \mathbf{F}^h the total force on the rod. Eq.(4) thus reduces to,

$$\mathbf{u}(\mathbf{r}) = - \frac{D}{L} \sum_{j=-n/2}^{n/2} \mathbf{T}(\mathbf{r} - \mathbf{r}_j) \cdot \mathbf{F}^h. \quad (6)$$

The force \mathbf{F}^h is calculated in terms of the translational velocity of the rod self-consistently from eq.(6) using Faxén’s theorem for translational motion for each spherical bead, where the velocity \mathbf{v}_j of bead j is expressed in terms of the force \mathbf{F}_j^h on bead j and the velocity $\mathbf{u}_0(\mathbf{r}_j)$ at the center of the bead that would have existed without that bead being present,

$$\mathbf{v}_j = - \frac{1}{3\pi\eta_0 D} \mathbf{F}_j^h + \mathbf{u}_0(\mathbf{r}_j) + \frac{1}{24} D^2 \nabla_j^2 \mathbf{u}_0(\mathbf{r}_j), \quad (7)$$

where ∇_j is the gradient operator with respect to \mathbf{r}_j . The first term on the right hand-side is just Stokes friction of a single bead in an unbounded fluid, while the second term accounts for hydrodynamic interaction between the beads. The fluid flow field \mathbf{u}_0 in turn is equal to,

$$\mathbf{u}_0(\mathbf{r}) = \sum_{i=-n/2, i \neq j}^{n/2} \oint_{\partial V_i} d\mathbf{S}' \mathbf{T}(\mathbf{r} - \mathbf{r}') \cdot \mathbf{f}_i^*(\mathbf{r}'), \quad (8)$$

where \mathbf{f}_i^* is the force per unit area that a surface element of bead i exerts on the fluid *in the absence of bead j* . For very long rods, consisting of many beads, the difference between \mathbf{f}_i (the corresponding force for the intact rod) and \mathbf{f}_i^* may be neglected: there are only a few neighbouring beads for which the difference is significant, but there are many more beads further away from bead j for which the difference is insignificant. To within the same approximations involved to arrive at eq.(4), eq.(8) can then be written as,

$$\mathbf{u}_0(\mathbf{r}_j) = - \sum_{i=-n/2, i \neq j}^{n/2} \mathbf{T}(\mathbf{r}_j - \mathbf{r}_i) \cdot \mathbf{F}_i^h. \quad (9)$$

Substitution of this expression into Faxén's theorem (7), and using that $\mathbf{r}_j - \mathbf{r}_i = (j - i)D\hat{\mathbf{u}}$, with $\hat{\mathbf{u}}$ the orientation of the rod, leads to,

$$\begin{aligned} \mathbf{v}_j = & -\frac{1}{3\pi\eta_0 D} \mathbf{F}_j^h - \frac{1}{8\pi\eta_0 D} \hat{\mathbf{u}}\hat{\mathbf{u}} \cdot \sum_{i=-n/2, i \neq j}^{n/2} \left[\frac{2}{|i-j|} - \frac{1}{6|i-j|^3} \right] \cdot \mathbf{F}_i^h \\ & - \frac{1}{8\pi\eta_0 D} [\hat{\mathbf{I}} - \hat{\mathbf{u}}\hat{\mathbf{u}}] \cdot \sum_{i=-n/2, i \neq j}^{n/2} \left[\frac{1}{|i-j|} + \frac{1}{12|i-j|^3} \right] \cdot \mathbf{F}_i^h, \end{aligned} \quad (10)$$

where eq.(3) has been used, together with,

$$\nabla^2 \mathbf{T}(\mathbf{r}) = \frac{1}{4\pi\eta_0 r^3} [\hat{\mathbf{I}} - 3\hat{\mathbf{r}}\hat{\mathbf{r}}]. \quad (11)$$

For pure translational motion, the velocity \mathbf{v}_j of each bead is equal to the velocity \mathbf{v} of the rod, so that both sides of eq.(10) can be summed over j , yielding for the left hand-side $\mathbf{v} L/D$. Neglecting end-effects and replacing sums by integrals (which is allowed for long and thin rods), it is found that,

$$\mathbf{v} = -\frac{\ln\{\mathbf{L}/\mathbf{D}\}}{4\pi\eta_0 \mathbf{L}} [\hat{\mathbf{I}} + \hat{\mathbf{u}}\hat{\mathbf{u}}] \cdot \mathbf{F}^h. \quad (12)$$

Notice that the Stokes friction contribution (the first term on the right hand-side in eq.(10)) is logarithmically small in comparison to the friction contribution due to hydrodynamic interaction between the beads. In fact, the Stokes contribution is neglected in eq.(12). A matrix inversion, in order to express \mathbf{F}^h in terms of \mathbf{v} , and subsequent substitution into eq.(6), after rewriting the sum over beads as an integral over the center line of the rod, yields,

$$\mathbf{u}(\mathbf{r}) = \frac{4\pi\eta_0}{\ln\{L/D\}} \int_{-L/2}^{L/2} dl \mathbf{T}(\mathbf{r} - \mathbf{r}_p - l\hat{\mathbf{u}}) \cdot \left[\hat{\mathbf{I}} - \frac{1}{2}\hat{\mathbf{u}}\hat{\mathbf{u}} \right] \cdot \mathbf{v}, \quad (13)$$

with \mathbf{r}_p the position coordinate of the rod. This is the approximate expression for the fluid flow generated by a translating long and thin rod that will be used in the following subsection to obtain an expression for the mobility matrices $\mathbf{M}_{1j}^{\mathbf{T}\mathbf{T}}$, $j = 1, 2$.

B. Calculation of $\mathbf{M}^{\mathbf{T}\mathbf{T}}$

In order to calculate the velocity \mathbf{v}_2 that rod 2 acquires in the flow field (13) generated by a translating rod 1, one should in principle perform a reflection calculation up to very high order : the field generated by rod 1 is scattered by each bead of rod 2 and subsequently reflected hence and forth between the different beads within rod 2. Such a calculation is hardly feasible analytically. Here, the field generated by rod 1 that is incident on rod 2 is approximated by a constant fluid flow field $\bar{\mathbf{u}}$ equal to the average of the incident field over the center line of rod 2. This "hydrodynamic mean-field approximation" is accurate for distances of the order L or larger, for which separations the incident field indeed becomes equal to a constant. For smaller distances between the rods this procedure provides a

semi-quantitative approximation. Within this approximation, the velocity of rod 2 immediately follows from eq.(12), with $\mathbf{v} = \mathbf{v}_2 - \bar{\mathbf{u}}$, $\mathbf{F}^h = \mathbf{F}_2^h$, the total force of the fluid on rod 2, and $\hat{\mathbf{u}} = \hat{\mathbf{u}}_2$, the orientation of rod 2,

$$\mathbf{v}_2 = \bar{\mathbf{u}} - \frac{\ln\{L/D\}}{4\pi\eta_0 L} \left[\hat{\mathbf{I}} + \hat{\mathbf{u}}_2 \hat{\mathbf{u}}_2 \right] \cdot \mathbf{F}_2^h. \quad (14)$$

The average incident flow field follows from eqs.(13) and (12), with $\mathbf{v} = \mathbf{v}_1$, the velocity of rod 1 and $\mathbf{F}^h = \mathbf{F}_1^h$, the force on rod 1,

$$\begin{aligned} \bar{\mathbf{u}} &= \frac{4\pi\eta_0 L}{\ln\{L/D\}} \mathbf{A} \cdot \left[\hat{\mathbf{I}} - \frac{1}{2} \hat{\mathbf{u}}_1 \hat{\mathbf{u}}_1 \right] \cdot \mathbf{v}_1 \\ &= -\mathbf{A} \cdot \left[\hat{\mathbf{I}} - \frac{1}{2} \hat{\mathbf{u}}_1 \hat{\mathbf{u}}_1 \right] \cdot \left[\hat{\mathbf{I}} + \hat{\mathbf{u}}_1 \hat{\mathbf{u}}_1 \right] \cdot \mathbf{F}_1^h \\ &= -\mathbf{A} \cdot \mathbf{F}_1^h, \end{aligned} \quad (15)$$

where,

$$\mathbf{A} = \frac{1}{L^2} \int_{-L/2}^{L/2} d\mathbf{l}_1 \int_{-L/2}^{L/2} d\mathbf{l}_2 \mathbf{T}(\mathbf{r}_{21} + l_2 \hat{\mathbf{u}}_2 - l_1 \hat{\mathbf{u}}_1), \quad (16)$$

with $\mathbf{r}_{21} = \mathbf{r}_2 - \mathbf{r}_1$ the distance between the centers of the two rods. Notice that for distances \mathbf{r}_{21} between the centers of the rods larger than L , the matrix \mathbf{A} asymptotes to $\mathbf{T}(\mathbf{r}_{21})$. By definition the following ‘‘mean-field’’ expressions for the translational mobility matrices are thus obtained (after an interchange of the indices 1 and 2),

$$\mathbf{M}_{11}^{\text{TT}} = \frac{\ln\{L/D\}}{4\pi\eta_0 L} \left[\hat{\mathbf{I}} + \hat{\mathbf{u}}_1 \hat{\mathbf{u}}_1 \right], \quad (17)$$

$$\mathbf{M}_{12}^{\text{TT}} = \frac{1}{L^2} \int_{-L/2}^{L/2} dl_1 \int_{-L/2}^{L/2} dl_2 \mathbf{T}(\mathbf{r}_{12} + l_1 \hat{\mathbf{u}}_1 - l_2 \hat{\mathbf{u}}_2). \quad (18)$$

One might try to devise approximate expressions for the matrix \mathbf{A} . However, sedimentation velocities are obtained as ensemble averages, also with respect to orientations, giving rise to integrals with respect to \mathbf{r}_{12} and $\hat{\mathbf{u}}_{1,2}$, which can be evaluated by numerical integration.

C. Concluding Remarks

The approximations involved in the above discussion are justified for very long rods, since $\mathcal{O}(1)$ -constants are neglected against terms of order $\ln\{L/D\}$, both by neglecting end-effects and replacing sums over beads by integrals (for the evaluation of the sums in Faxén’s theorem in eq.(10)). Such approximations are most important for the diagonal mobility matrix $\mathbf{M}_{11}^{\text{TT}}$ (notice that factors $\ln\{L/D\}$ do not appear in the off-diagonal matrix $\mathbf{M}_{12}^{\text{TT}}$, due to the resubstitution of velocities in terms of forces). Both end-effects and the mathematical approximations involved in the calculation of the diagonal mobility matrix $\mathbf{M}_{11}^{\text{TT}}$ in eq.(17) may be accurately accounted for by the replacement,

$$\ln\{L/D\} \rightarrow \ln\{L/D\} - \nu, \quad (19)$$

with $\nu = \nu_\perp$ and $\nu = \nu_\parallel$ a constant, pertaining to translational motion perpendicular and parallel to the rods orientation, respectively. This correction is experimentally significant for somewhat shorter rods ($L/D < 20$, say), but vanishes relatively to the logarithmic term for very long rods. The actual values of ν_\perp and ν_\parallel for cylindrical rods are equal to [4],

$$\nu_\perp = -0.84, \quad (20)$$

$$\nu_\parallel = 0.21. \quad (21)$$

A more accurate expression for $\mathbf{M}_{11}^{\text{TT}}$ than in eq.(17) is,

$$\mathbf{M}_{11}^{\text{TT}} = \frac{\ln\{L/D\}}{4\pi\eta_0 L} \left[\hat{\mathbf{I}} + \hat{\mathbf{u}}_1 \hat{\mathbf{u}}_1 \right] - \frac{1}{4\pi\eta_0 L} \left[\nu_\perp \hat{\mathbf{I}} + (2\nu_\parallel - \nu_\perp) \hat{\mathbf{u}}_1 \hat{\mathbf{u}}_1 \right]. \quad (22)$$

In the sequel we will use this expression for the mobility matrix $\mathbf{M}_{11}^{\text{TT}}$ instead of eq.(17). The approximations involved in the off-diagonal mobility matrices in eqs.(34,38) are primarily due to the mean-field treatment of the incident flow field. It is probably a formidable task to improve on these expressions.

The use of the more accurate expression (22) for the diagonal translational mobility matrix also circumvents the practical problem of calculating volume fractions of colloidal rod material from given values for L , D and number density. For the bead model it is not so clear how the volume of a rod must be expressed in terms of L and D . The volume of the cylindrical rod is simply equal to $\frac{\pi}{4}D^2L$.

III. AN EXPRESSION FOR THE SEDIMENTATION VELOCITY OF RODS

The sedimentation of colloidal material induces, through the presence of the walls of the container, backflow of solvent. The backflow velocity is inhomogeneous, and varies on the length scale of the container. On a local scale, however, the backflow may be considered homogeneous, and the sedimentation velocity can be calculated relative to the local backflow velocity. This *relative* sedimentation velocity is a constant throughout the container (except possibly in a small region of extent L near the walls of the container, where gradients of the backflow velocity are large), and depends only on the properties of the suspension. A formal evaluation of the sedimentation velocity directly from eq.(1), by ensemble averaging, leads to spurious divergences, which are the result of the neglect of the hydrodynamic effects of the walls of the container which lead to solvent backflow. Batchelor was the first to deal with these divergences correctly, and we will use his arguments here [2].

Ensemble averaging of \mathbf{v}_1 in eq.(1) gives the sedimentation velocity \mathbf{v}_s , which is thus found to be equal to,

$$\mathbf{v}_s = - \langle \mathbf{M}_{11}^{\text{TT}} \cdot \mathbf{F}_1^h + \bar{\rho} \mathbf{V} \mathbf{M}_{12}^{\text{TT}} \cdot \mathbf{F}_2^h + \mathbf{M}_{11}^{\text{TR}} \cdot \mathbf{T}_1^h + \bar{\rho} \mathbf{V} \mathbf{M}_{12}^{\text{TR}} \cdot \mathbf{T}_2^h \rangle, \quad (23)$$

where the brackets $\langle \dots \rangle$ denote ensemble averaging with respect to positions and orientations of the rods. The factors $\bar{\rho}V = N \approx N-1$ account for the presence of $N-1$ rods which all interact with rod 1 under consideration. The divergence problems mentioned above arising in the explicit evaluation of the ensemble averages will be dealt with later.

In order to be able to calculate these ensemble averages, the forces and torques must be expressed in terms of the positions and orientations of the rods. On the Brownian time scale there is a balance between all the forces and torques on each of the rods, that is, the total force and torque are equal to zero. The total force in turn is equal to the sum of the force \mathbf{F}_j^h that the fluid exerts on the rod, the interaction force $\mathbf{F}_j^I = -\nabla_j \Phi$ (with Φ the total interaction energy of the rods), the Brownian force $\mathbf{F}_j^{Br} = -k_B T \nabla_j \ln\{P\}$ (with k_B Boltzmann's constant, T the temperature and P the probability density function for positions and orientations), and the external force \mathbf{F}^{ext} due to the gravitational field. Hence,

$$\mathbf{F}_j^h = \nabla_j \Phi + k_B T \nabla_j \ln\{P\} - \mathbf{F}^{ext}. \quad (24)$$

Similarly, the total torque is the sum of the hydrodynamic torque \mathbf{T}_j^h , the interaction torque $-\hat{\mathcal{R}}_j \Phi$, the Brownian torque $-k_B T \hat{\mathcal{R}}_j \ln\{P\}$, while the torque on each rod due to the homogeneous external force vanishes. Hence,

$$\mathbf{T}_j^h = \hat{\mathcal{R}}_j \Phi + k_B T \hat{\mathcal{R}}_j \ln\{P\}, \quad (25)$$

where the rotation operator is defined as,

$$\hat{\mathcal{R}}_j(\dots) \equiv \hat{\mathbf{u}}_j \times \nabla_{u_j}(\dots), \quad (26)$$

with ∇_{u_j} the gradient operator with respect to $\hat{\mathbf{u}}_j$. Substitution of eqs.(24,25) into eq.(23) for the sedimentation velocity yields,

$$\begin{aligned} \mathbf{v}_s = - \langle & \mathbf{M}_{11}^{\text{TT}} \cdot [\nabla_1 \Phi + \mathbf{k}_B \mathbf{T} \nabla_1 \ln\{\mathbf{P}\} - \mathbf{F}^{ext}] \\ & \bar{\rho} \mathbf{V} \mathbf{M}_{12}^{\text{TT}} \cdot [\nabla_2 \Phi + \mathbf{k}_B \mathbf{T} \nabla_2 \ln\{\mathbf{P}\} - \mathbf{F}^{ext}] \\ & + \mathbf{M}_{11}^{\text{TR}} \cdot [\hat{\mathcal{R}}_1 \Phi + \mathbf{k}_B \mathbf{T} \hat{\mathcal{R}}_1 \ln\{\mathbf{P}\}] + \bar{\rho} \mathbf{V} \mathbf{M}_{12}^{\text{TR}} \cdot [\hat{\mathcal{R}}_2 \Phi + \mathbf{k}_B \mathbf{T} \hat{\mathcal{R}}_2 \ln\{\mathbf{P}\}] \rangle. \end{aligned} \quad (27)$$

The next step in the explicit evaluation of these ensemble averages is to determine the stationary probability density function $P \equiv P(\mathbf{r}_1, \mathbf{r}_2, \hat{\mathbf{u}}_1, \hat{\mathbf{u}}_2)$ for the positions and orientations of two rods. At this point it is convenient to introduce the pair-correlation function g , defined as,

$$P(\mathbf{r}_1, \mathbf{r}_2, \hat{\mathbf{u}}_1, \hat{\mathbf{u}}_2) \equiv P(\mathbf{r}_1, \hat{\mathbf{u}}_1) P(\mathbf{r}_2, \hat{\mathbf{u}}_2) g(\mathbf{r}_{12}, \hat{\mathbf{u}}_1, \hat{\mathbf{u}}_2), \quad (28)$$

where $P(\mathbf{r}_j, \hat{\mathbf{u}}_j)$ is the probability density function for the position and orientation of a single rod. For spherical particles in a homogeneous external gravitational field, the probability density function for the position coordinates is simply the equilibrium function, without an external field, provided that the particles are identical. The probability density function differs from the equilibrium function only in case the relative sedimentation velocity of two spheres is different, for example due to differing masses and/or sizes. For rods, things are somewhat more complicated. Even if two rods are identical their relative sedimentation velocity generally differs as a result of the fact that the translational friction constant of rods is orientation dependent (see eq.(17)). The probability density function is generally dependent on the external force due to the fact that rods with different orientations overtake each other during sedimentation. Suppose, however, that the sedimentation velocity is so slow, that during a relative displacement of two rods in the gravitational field of the order of the length L of the rods, each rod rotated many times due to their Brownian motion. The relative sedimentation velocity of two rods then averages out to zero. For such a case, the pair-correlation function is only weakly perturbed by the external field, so that we may use its equilibrium Boltzmann form,

$$g(\mathbf{r}_1, \mathbf{r}_2, \mathbf{u}_1, \mathbf{u}_2) = \exp\{-\beta\Phi(\mathbf{r}_1, \mathbf{r}_2, \hat{\mathbf{u}}_1, \hat{\mathbf{u}}_2)\}, \quad (29)$$

Let us derive the inequality that should be satisfied for eq.(29) to be valid. According to eq.(17), the largest relative sedimentation velocity $|\Delta\mathbf{v}_s|$ of two rods is approximately equal to,

$$|\Delta\mathbf{v}_s| \approx \frac{\ln\{L/D\}}{4\pi\eta_0 L} |\mathbf{F}^{ext}|. \quad (30)$$

On the other hand, the time τ_{rot} required for a rotational revolution is equal to,

$$\tau_{rot} = \frac{\pi\eta_0 L^3}{3k_B T \ln\{L/D\}}. \quad (31)$$

The condition under which eq.(29) for the pair-correlation function is a good approximation is therefore,

$$\frac{L/|\Delta\mathbf{v}_s|}{\tau_{rot}} \approx \frac{12k_B T}{|\mathbf{F}^{ext}| L} \gg 1. \quad (32)$$

Hence, the work provided by the external force to displace a colloidal rod over a distance equal to its length should be much smaller than a few times the thermal energy of the rods. Substitution of typical numbers shows that this inequality is satisfied under normal practical circumstances.¹ Furthermore, when alignment of the rods during sedimentation in a homogeneous suspension is of no importance, the one-particle probability density functions in eq.(28) are both constants equal to,

$$P(\mathbf{r}_j, \hat{\mathbf{u}}_j) = \frac{1}{4\pi V}. \quad (33)$$

We will restrict ourselves here to the most common situation where the inequality (32) is satisfied, and assume negligible alignment, so that the probability density function is well approximated by eqs.(28,29,33). In that case many of the terms in eq.(27) for the sedimentation velocity cancel : the interaction contributions cancel against the Brownian terms. The sedimentation velocity reduces simply to,

$$\mathbf{v}_s = [\langle \mathbf{M}_{11}^{\mathbf{T}\mathbf{T}} \rangle + \bar{\rho} \mathbf{V} \langle \mathbf{M}_{12}^{\mathbf{T}\mathbf{T}} \rangle] \cdot \mathbf{F}^{ext}. \quad (34)$$

Since $\mathbf{M}_{12}^{\mathbf{T}\mathbf{T}}(\mathbf{r}_{12}, \hat{\mathbf{u}}_1, \hat{\mathbf{u}}_2) \sim \mathbf{1}/\mathbf{r}_{12}$ for large distances, its ensemble average with respect to position coordinates diverges. Such a spurious divergence is also found for spherical particles, and is the result of the neglect of the hydrodynamic effect of the walls of the container. Batchelor [2] showed that a formally divergent quantity, which is unambiguously finite valued on physical grounds, can be subtracted from the ensemble average, rendering a perfectly well defined sedimentation velocity. This finite valued quantity is formally divergent for the same reason that the ensemble average

¹ For example, for rods with a length of 100 nm, the sedimentation velocity should be much less than 1 mm/min, in order that the inequality (32) is satisfied.

of $\mathbf{M}_{12}^{\mathbf{T}\mathbf{T}}$ is divergent, and subtraction accounts for the local hydrodynamic effects of the wall.² Batchelor's argument is as follows. First define the velocity $\mathbf{u}(\mathbf{r} | \mathbf{r}_1, \dots, \mathbf{r}_N, \hat{\mathbf{u}}_1, \dots, \hat{\mathbf{u}}_N)$ as the velocity at a point \mathbf{r} (either in the fluid or inside a colloidal rod), given the positions $\mathbf{r}_1, \dots, \mathbf{r}_N$ and orientations $\hat{\mathbf{u}}_1, \dots, \hat{\mathbf{u}}_N$ of N rods. In the laboratory reference frame the net flux of material through a cross sectional area must be zero. This means that the ensemble average of \mathbf{u} must be zero. Hence,

$$\begin{aligned} \mathbf{0} &= \langle \mathbf{u}(\mathbf{r} | \mathbf{r}_1, \dots, \mathbf{r}_N, \hat{\mathbf{u}}_1, \dots, \hat{\mathbf{u}}_N) \rangle \\ &= \int d\mathbf{r}_1 \dots \int d\mathbf{r}_N \oint d\hat{\mathbf{u}}_1 \dots \oint d\hat{\mathbf{u}}_N \mathbf{u}(\mathbf{r} | \mathbf{r}_1, \dots, \mathbf{r}_N, \hat{\mathbf{u}}_1, \dots, \hat{\mathbf{u}}_N) \mathbf{P}(\mathbf{r}_1, \dots, \mathbf{r}_N, \hat{\mathbf{u}}_1, \dots, \hat{\mathbf{u}}_N), \end{aligned} \quad (35)$$

where $P(\mathbf{r}_1, \dots, \hat{\mathbf{u}}_N)$ is the probability density function for $\{\mathbf{r}_1, \dots, \hat{\mathbf{u}}_N\}$. Formally, this ensemble average diverges for the same reason that the sedimentation velocity diverges : the flow field \mathbf{u} varies like $1/r$ for large distances due to its Oseen contribution. The formally divergent expression (35), that must be zero for physical reasons, is subtracted from eq.(34) for the sedimentation velocity to render this expression convergent. The field \mathbf{u} can generally be written as the sum of a two terms : a term to which the field would be equal to in the absence of reflection contributions plus a term that accounts for the reflection contributions. To within our approach reflection contributions are neglected so that only the former term survives here. Hence,

$$\begin{aligned} \mathbf{u}(\mathbf{r} | \mathbf{r}_1, \dots, \mathbf{r}_N, \hat{\mathbf{u}}_1, \dots, \hat{\mathbf{u}}_N) &= \sum_{j=1}^N \mathbf{u}(\mathbf{r} - \mathbf{r}_j) \quad , \quad \text{for } \mathbf{r} \text{ in the fluid,} \\ &= \mathbf{v}_s \quad , \quad \text{for } \mathbf{r} \text{ in a core,} \end{aligned} \quad (36)$$

where the field $\mathbf{u}(\mathbf{r} - \mathbf{r}_j)$, for \mathbf{r} in the fluid, is the sum of the flow fields in eq.(13), (with \mathbf{v} replaced by $\mathbf{v}_s - \mathbf{u}_s$), and eq.(66) in appendix A, (both considered as a function of the relative distance to the j^{th} rod under consideration), that is,

$$\mathbf{u}(\mathbf{r} - \mathbf{r}_j) = \mathbf{u}_T(\mathbf{r} - \mathbf{r}_j) + \mathbf{u}_R(\mathbf{r} - \mathbf{r}_j), \quad (37)$$

where $\mathbf{u}_T(\mathbf{r} - \mathbf{r}_j)$ is the fluid flow generated by a translating rod as given in eq.(13),

$$\mathbf{u}_T(\mathbf{r} - \mathbf{r}_j) = \frac{1}{L} \int_{-L/2}^{L/2} dl_j \mathbf{T}(\mathbf{r} - \mathbf{r}_j - l_j \hat{\mathbf{u}}_j) \cdot \mathbf{F}^{ext}, \quad (38)$$

where the inverse of eq.(12) is used, together with $\mathbf{F}^h = -\mathbf{F}^{ext}$, and $\mathbf{u}_R(\mathbf{r} - \mathbf{r}_j)$ is the field generated by a rotating rod, which is similarly given by eq.(66) in appendix A. Operating on both sides of eq.(35) with $\int d\mathbf{r} \oint d\hat{\mathbf{u}} P(\mathbf{r}, \hat{\mathbf{u}})$, where $P(\mathbf{r}, \hat{\mathbf{u}})$ is the constant specified in eq.(33), and subtraction of the resulting equation from eq.(34) for the sedimentation velocity yields, for identical rods and to first order in concentration (rename $\mathbf{r}_1 = \mathbf{r}_2$, $\mathbf{r} = \mathbf{r}_1$, $\hat{\mathbf{u}}_1 = \hat{\mathbf{u}}_2$ and $\hat{\mathbf{u}} = \hat{\mathbf{u}}_1$),

$$\begin{aligned} \mathbf{v}_s &= -\varphi \mathbf{v}_s + [\langle \mathbf{M}_{11}^{\mathbf{T}\mathbf{T}} \rangle + \bar{\rho} \mathbf{V} \langle \mathbf{M}_{12}^{\mathbf{T}\mathbf{T}} \rangle] \cdot \mathbf{F}^{ext} \\ &\quad - \frac{\bar{\rho}}{(4\pi)^2} \int d\mathbf{r}_{12} \oint d\hat{\mathbf{u}}_1 \oint d\hat{\mathbf{u}}_2 [\mathbf{u}_T(\mathbf{r}_{12}) + \mathbf{u}_R(\mathbf{r}_{12})] \chi_f(\mathbf{r}_1 | \mathbf{r}_2, \hat{\mathbf{u}}_2), \end{aligned} \quad (39)$$

where χ_f is the characteristic function that restricts the integrations to points \mathbf{r} which are in the fluid, not inside the core of rod 2,

$$\begin{aligned} \chi_f(\mathbf{r} | \mathbf{r}_2, \hat{\mathbf{u}}_2) &= 1 \quad , \quad \text{for } \mathbf{r} \text{ in the fluid,} \\ &= 0 \quad , \quad \text{for } \mathbf{r} \text{ in the core of rod 2.} \end{aligned} \quad (40)$$

Without interactions the angular velocity of each rod is simply proportional to the hydrodynamic torque on the same rod (see eqs.(59,64) in appendix A), which hydrodynamic torques are zero. Since the integral in the above expression

² To within the approximations made here, valid for long and thin rods, we do not encounter a conditionally divergent contribution due to terms $\sim 1/r_{12}^3$, as for spheres. Such a divergence can be dealt with by noting that the ensemble average of the deviatoric part of the stress tensor vanishes. We will not go into the extension of Batchelor's arguments to rods to deal with this conditionally divergence problem.

for the sedimentation velocity is multiplied by the concentration $\bar{\rho}$, it follows that the rotational field \mathbf{u}_R does not contribute to first order in the density. For the same reason, in each term that is multiplied by the concentration, \mathbf{F}^{ext} may be expressed with eq.(22) in terms of the sedimentation velocity \mathbf{v}_s^0 without interactions, at infinite dilution, as,

$$\mathbf{v}_s^0 = \left[\frac{\ln\{L/D\}}{3\pi\eta_0 L} - \frac{1}{6\pi\eta_0 L}(\nu_\perp + \nu_\parallel) \right] \mathbf{F}^{ext}. \quad (41)$$

We thus find the following expression for the sedimentation velocity, valid to first order in volume fraction,

$$\mathbf{v}_s = \mathbf{v}_s^0 \left[1 - \left(\frac{f_1 + f_2}{2\ln\{L/D\} - (\nu_\perp + \nu_\parallel)} + \mathcal{O}(\mathcal{D}/\mathcal{L}) \right) \frac{L}{D} \varphi \right], \quad (42)$$

where the functions f_1 and f_2 are equal to,

$$f_1 = -\frac{1}{4\pi^3 DL^3} \int d\mathbf{r}_{12} \oint d\hat{\mathbf{u}}_1 \oint d\hat{\mathbf{u}}_2 [g(\mathbf{r}_{12}, \hat{\mathbf{u}}_1, \hat{\mathbf{u}}_2) - \chi_f(\mathbf{r}_1 | \mathbf{r}_2, \hat{\mathbf{u}}_2)] \\ \times \int_{-L/2}^{L/2} dl_1 \int_{-L/2}^{L/2} dl_2 \frac{1}{|\mathbf{r}_{12} + l_1 \hat{\mathbf{u}}_1 - l_2 \hat{\mathbf{u}}_2|}, \quad (43)$$

$$f_2 = -\frac{1}{4\pi^3 DL^3} \int d\mathbf{r}_{12} \oint d\hat{\mathbf{u}}_1 \oint d\hat{\mathbf{u}}_2 \chi_f(\mathbf{r}_1 | \mathbf{r}_2, \hat{\mathbf{u}}_2) \\ \times \int_{-L/2}^{L/2} dl_1 \int_{-L/2}^{L/2} dl_2 \left[\frac{1}{|\mathbf{r}_{12} + l_1 \hat{\mathbf{u}}_1 - l_2 \hat{\mathbf{u}}_2|} - \frac{1}{|\mathbf{r}_{12} - l_2 \hat{\mathbf{u}}_2|} \right]. \quad (44)$$

where the expressions (13) and (38) for the mobility matrix $\mathbf{M}_{12}^{\mathbf{T}\mathbf{T}}$ and the field \mathbf{u}_T are used, respectively. We also used that integrals over the Oseen tensor must be proportional to the identity tensor, so that in these integrals the Oseen tensor may be replaced by the trace $\frac{1}{3}Tr\{\mathbf{T}\}$ of that tensor, which, according to its defining equation (3), is equal to,

$$Tr\{\mathbf{T}(\mathbf{r})\} = \frac{1}{2\pi\eta_0 r}. \quad (45)$$

For rods interacting only via a hard-core repulsion, it is shown in appendix B how to reduce the number of integrations, leading to the following results,

$$f_1 = \frac{8}{\pi^3} \int_0^\infty dx \int_{-1}^1 dz_1 \int_{-1}^1 dz_2 \int_0^\pi d\Psi \\ \times j_0^2(x z_1) j_0^2(x z_2) \left[1 - \left(z_1 z_2 + \sqrt{(1 - z_1^2)(1 - z_2^2)} \cos\{\Psi\} \right)^2 \right]^{1/2} + \mathcal{O}(\mathcal{D}/\mathcal{L}) \\ = 6.4 \dots + \mathcal{O}(\mathcal{D}/\mathcal{L}), \quad (46)$$

$$f_2 = \frac{2}{9} \frac{L}{D} + \mathcal{O}(\mathcal{D}/\mathcal{L}). \quad (47)$$

The numerical value for f_1 has been obtained by numerical integration and applies for hard-core interactions, where g is equal to 0 when two cores overlap, and equal to 1 otherwise. The result for f_2 is independent of the kind of direct interaction between the rods.

Substitution of the numerical values for f_1 and f_2 from eqs.(46,47) and into eq.(42) gives our final result for the sedimentation velocity up to $\mathcal{O}(\mathcal{D}/\mathcal{L})$ contributions,

$$\mathbf{v}_s = \mathbf{v}_s^0 \left[1 - \frac{6.4 + \frac{2}{9} \frac{L}{D}}{2\ln\{L/D\} - (\nu_\perp + \nu_\parallel)} \frac{L}{D} \varphi \right], \quad (48)$$

The volume fraction prefactor,

$$\alpha = \frac{6.4 + \frac{2}{9} \frac{L}{D}}{2\ln\{L/D\} - (\nu_\perp + \nu_\parallel)} \frac{L}{D}, \quad (49)$$

is plotted as a function of L/D in Fig.1 (where both ν_{\perp} and ν_{\parallel} are taken equal to 0). Also plotted is an older result due to Peterson [3] who predicted,

$$\alpha = \frac{8(3/8)^{2/3}(L/D)^{1/3}}{2\ln\{L/D\}} \frac{L}{D}. \quad (50)$$

In this latter theory back flow is not correctly accounted for, hydrodynamic interactions are orientationally preaveraged and certain integrals are not precisely calculated but only estimated. The data points shown in Fig. 1a are experimental results for silica rods, coated with stearyl alcohol and dissolved in cyclohexane. The data point \times is taken from Ref. [5]. The point \circ is an unpublished result from the same author's. The data point in Fig. 1b is a data point for *fd*-virus at high salt concentration, as obtained in the experimental section of the present paper. As can be seen from Fig. 1, the present prediction is virtually equal to that of Peterson for $L/D < 30$, but large differences are found for large aspect ratios. For large aspect ratios, α is predicted to vary like $\sim (L/D)^2 / \ln\{L/D\}$, in contrast to Peterson's result $\sim (L/D)^{4/3} / \ln\{L/D\}$. For smaller aspect ratios α approaches approximately Batchelor's value for spheres $\alpha = 6.55$, which is probably fortuitous in view of the approximations made here which limit the results to be meaningful only for long and thin rods.

IV. EXPERIMENTAL RESULTS

The concentration dependence of the sedimentation velocity predicted by Eq. (49) differs significantly from Peterson's result Eq. (50) only for rods with large L/D . In our experiments we have used filamentous bacteriophage *fd* which is a rod-like virus with $L/D \approx 130$. Other relevant physical characteristics of *fd*, are its length $L = 880\text{nm}$, its diameter $D = 6.6\text{ nm}$ [6], and its density of 1.285 mg/ml [7]. Because of its large L/D ratio the virus is a semi-flexible rather than a rigid rod characterized with persistence length of $2.2\text{ }\mu\text{m}$ [8]. Its linear charge density is $10\text{ e}^-/\text{nm}$ at pH 8.2 [9].

We have grown *fd* virus according to standard procedures of molecular biology described in Maniatis [10]. The virus suspension was first purified in a cesium chloride density gradient and then extensively dialyzed against tris buffer at pH 8.15 and at the desired ionic strength for the sedimentation experiments. After that the virus was concentrated by ultracentrifugation and from this stock solution a series of samples with different concentrations were prepared. The sedimentation velocity was measured on a Beckman XL-A analytical ultracentrifuge equipped with UV absorbance optics. Most of the experiments were done at $25\text{ }^{\circ}\text{C}$ and at a centrifugal force equal to $45,500\text{ g's}$ ($25,000\text{ rpm}$). Before each sedimentation experiment the sample and rotor were allowed to equilibrate at the desired temperature for a few hours. Sedimentation data showed some unexpected features, interfering with straightforward calculation of the sedimentation coefficient. For this reason we have added appendix C, where the detailed analysis of our data is given.

The measured sedimentation velocity for a range of volume fractions of *fd* from dilute solution up to a stable nematic phase are shown in Fig. 2. All the samples in these measurements were kept at 8mM ionic strength. The sedimentation velocity of rods in the isotropic phase uniformly decreases with increasing concentration. After Ref. [10] we have tried to fit our experimental data to a functional form $S_{\phi} = S_0(1 - p\phi)^{\nu}$ where S_0 is the sedimentation velocity at infinite dilution and ϕ is the volume fraction of rods. The experimental values of sedimentation velocity are reported in Svedbergs where $1\text{ S} = 10^{-13}\text{ s}^{-1}$. As seen from Fig. 2 we obtain a reasonable fit to the experimental data in the isotropic phase and find that the sedimentation velocity at infinite dilution is $S_0 = 46.0$ for the value of constants $\nu = -1/3$ and $p=3600$. After linearizing our fitted formula we find that the volume prefactor $\alpha \approx 1200$ is much larger than predicted by Eq. (49). The reason for such a high value of slope α is the low ionic strength at which the experiment was performed. The same increase in α with decreasing ionic strength is observed in sedimentation of spherical particles [12,13]. Also we note that in this case the region where the sedimentation velocity varies linearly with rod concentration is limited to very low volume fraction of rods.

It is a well known fact that elongated rods at high volume fractions undergo a first order phase transition to a liquid crystalline nematic phase [14]. The nematic phase is characterized by a short range liquid-like positional order and long range solid-like orientational order of rods. *fd* virus forms a cholesteric phase instead of the nematic phase [6,15]. Locally the cholesteric phase is equivalent to nematic, however on a macroscopic scale the average direction of molecules in a cholesteric phase forms a helix. The free energy difference between a cholesteric phase and a nematic phase is very small and although our experiments are performed on the cholesteric phase only, we expect that our results are generic and would hold for a nematic phase of hard rods as well.

Bacteriophage *fd* in the cholesteric phase exhibits qualitatively new behavior when placed in centrifugal field. Instead of a single sedimenting boundary and single plateau we observe two boundaries with two plateau's sedimenting at different velocities as shown in Fig. 3. To confirm that this change in sedimentation behavior is indeed due to the formation of the nematic phase we have made a sample which is co-existing between the isotropic and nematic phase. After the sample had phase separated into macroscopically distinct co-existing phases, each phase was sedimented separately. In the isotropic phase there was no sign of a second boundary, while in the nematic (cholesteric) phase we observed a fast sedimenting second boundary that was slightly more concentrated than the first component. On one hand, the slow component had a plateau concentration and a sedimentation velocity that was almost independent of the average concentration. On the other hand, the sedimentation velocity of the faster moving component rapidly decreases with increasing *fd* concentration and at the same time the difference between the plateau concentrations of the two components increases with increasing average concentration.

The unstable sedimentation of colloidal rods in the nematic phase has a similar origin as the self-sharpening effect described in Appendix C. The reason for the instability is the discontinuous jump in sedimentation velocity that occurs at the isotropic-nematic phase transition as is shown in Fig. 2 [16]. The denser nematic phase sediments at a significantly higher velocity than a more dilute isotropic phase. Initially a stable nematic phase occupies the whole sample length. When the centrifugal field is turned on a sharp sedimenting boundary starts moving towards the bottom of the container. Below this boundary (to the right) the rods are still in the nematic phase while above it the concentration of rods is very low and therefore they are in the isotropic state. This occurs because some particles will inevitably diffuse against the centrifugal field from a highly concentrated plateau into the dilute region. As this happens they simultaneously undergo a transition from the nematic to the isotropic phase. Since the sedimentation velocity of rods in the isotropic phase is much lower than in nematic phase, the probability of the rods diffusing from the isotropic phase back into the nematic phase is virtually zero. It is this asymmetry that results in a continuous flux of particles from the nematic into the isotropic phase and contributes to the formation of the second plateau in the isotropic phase that is moving at a slower speed. The concentration of the rods in the isotropic plateau will be very close to the concentration of isotropic rods co-existing with the nematic phase due to the self-sharpening effect because dilute isotropic rods will catch up with more concentrated isotropic rods. However, the highest concentration the isotropic rods can attain is the co-existence concentration between the isotropic and nematic phases, as long as the nematic phase sediments faster than the isotropic phase. Indeed, this is very close to what we observe in Fig. 3. Another experimental observation corroborating our explanation is that the sedimentation velocity and concentration of the slower isotropic plateau does not change significantly with average concentration of rods as seen in Fig 2.

Since the theory presented in this paper is valid only to first order in concentration of rods, to obtain an accurate value of the prefactor α in Eq. 49 we have made additional measurements in the dilute to semi-dilute range. Our results are presented in Fig. 4. We note that the overlap to semi-dilute concentration for *fd* with $L = 0.88\mu\text{m}$ is at volume fraction of $5.9 \cdot 10^{-5}$. Unlike the previous measurements, we have done these measurements at high ionic strength where the behavior of charged rods is expected to approach the behavior of hard rods. Additionally at high ionic strength we expect the sedimentation velocity to have a linear dependence on volume fraction of rods up to higher values of volume fraction. The results for ionic strength of 50mM and 100mM ionic strength are shown in figure 4. The volume prefactor in Eq. (49) at 50 mM ionic strength is $\alpha = 450 \pm 40$ and at 100mM ionic strength $\alpha = 440 \pm 60$. We have repeated the experiment at 100mM ionic strength on a different analytical Beckman X1-A ultracentrifuge and obtained the following result $\alpha = 490 \pm 50$. We conclude that $\alpha = 470 \pm 50$ which is the result plotted in Fig. 1b. Since the values of the coefficient α do not change much with changing ionic strength from 50 mM to 100mM we conclude that the charged rods have approached the hard rod limit. Note that because of its large L/D ratio *fd* is slightly flexible with a persistence length which is 2.5 times its contour length [7]. Still for the experimentally determined parameters of *fd*, which are $L = 880\text{nm}$ and $D = 6.6\text{nm}$, our experimental results compare favorably to the Eq. 49, which predicts the value of $\alpha = 488$ (see Fig. 1). In contrast, the previous result due to Peterson in Eq. 50 predicts a lower value of $\alpha = 288$

V. ACKNOWLEDGMENT

We acknowledge valuable discussions with R. B. Meyer. This research was supported by National Science Foundations grants No. DMR-9705336, INT-9113312 and by the Netherlands Foundations of Fundamental Research(FOM). Additional information is available online: www.elsie.brandeis.edu.

APPENDIX A

Flow field generated by a rotating rod

Consider a rod with its center at the origin, which rotates with an angular velocity $\boldsymbol{\Omega}$. The angular velocity is decomposed in its component perpendicular and parallel to the rods center line,

$$\boldsymbol{\Omega}_\perp = \left[\hat{\mathbf{I}} - \hat{\mathbf{u}}\hat{\mathbf{u}} \right] \cdot \boldsymbol{\Omega}, \quad (51)$$

$$\boldsymbol{\Omega}_\parallel = \hat{\mathbf{u}} \cdot \boldsymbol{\Omega}. \quad (52)$$

Due to the linearity of the governing hydrodynamic equations, the flow fields generated by a rod rotating along $\boldsymbol{\Omega}_\perp$ and $\boldsymbol{\Omega}_\parallel$ may be calculated separately and added to obtain the flow field of the rod rotating along $\boldsymbol{\Omega}$.

Let us first consider a rod rotating with an angular velocity $\boldsymbol{\Omega}_\perp$. The flow field that is generated by this rotating rod is given by the general equation (2). The relative change of the velocity of the beads is $\sim 1/j$. For beads further away from the origin one may therefore consider the velocity over larger groups of beads as being virtually constant. The force on bead j is then proportional to its own velocity,

$$\mathbf{F}_j^h = -C \boldsymbol{\Omega}_\perp \times \mathbf{r}_j = -C D \mathbf{j} \boldsymbol{\Omega}_\perp \times \hat{\mathbf{u}}. \quad (53)$$

where C is an as yet unknown proportionality constant. This expression is not valid for beads close to the center of the rod : for these beads the forces may have a different direction than their velocity. The fluid flow field generated by a long and thin rod, however, is primarily determined by the relatively large velocities of the beads further away from its center. We may therefore use eq.(53), except for relatively few beads close to the center and near the tips of the rod. Since $\mathbf{r}_j = jD\hat{\mathbf{u}}$, the torque is thus found, to leading order in D/L , to be equal to,

$$\mathbf{T}_\perp^h = \sum_{j=-n/2}^{n/2} \mathbf{r}_j \times \mathbf{F}_j^h = -C D^2 \frac{1}{12} \left(\frac{L}{D} \right)^3 \hat{\mathbf{u}} \times (\boldsymbol{\Omega}_\perp \times \hat{\mathbf{u}}) = -C D^2 \frac{1}{12} \left(\frac{L}{D} \right)^3 \boldsymbol{\Omega}_\perp, \quad (54)$$

since $\boldsymbol{\Omega}_\perp$ is perpendicular to $\hat{\mathbf{u}}$. It is used here that $\sum_{j=1}^k j^2 = \frac{1}{6}k(k+1)(2k+1)$. First of all, the constant C is calculated self-consistently from Faxén's theorem in the form of eq.(10). Multiplying both sides of eq.(10) by $\mathbf{r}_j \times$, using that $\mathbf{r}_j \times \mathbf{v}_j = j^2 D^2 \boldsymbol{\Omega}_\perp$, and summation over beads, leads to,

$$\frac{1}{12} \left(\frac{L}{D} \right)^3 D^2 \boldsymbol{\Omega}_\perp = -\frac{1}{3\pi\eta_0 D} \mathbf{T}_\perp^h + \frac{C D}{8\pi\eta_0} \left(\frac{L}{D} \right)^3 g(L/D) \boldsymbol{\Omega}_\perp, \quad (55)$$

where the function g is defined as,

$$g(L/D) = \frac{1}{(n+1)^3} \sum_{j=-n/2}^{n/2} \sum_{i=-n/2, i \neq j}^{n/2} ij \left[\frac{1}{|i-j|} + \frac{1}{12} \frac{1}{|i-j|^3} \right]. \quad (56)$$

For long and thin rods the summations may be replaced by integrals, leading to,

$$g(L/D) = \frac{1}{6} \ln\{L/D\}, \quad (57)$$

up to leading order in D/L . Substitution of eq.(17) for the torque yields a single equation for C , yielding, again up to leading order,

$$C = \frac{4\pi\eta_0 D}{\ln\{L/D\}}. \quad (58)$$

Hence, from eq.(17),

$$\boldsymbol{\Omega}_\perp = -\frac{3 \ln\{L/D\}}{\pi\eta_0 L^3} \mathbf{T}_\perp^h. \quad (59)$$

The flow field \mathbf{u}_\perp that is generated by a rotating rod may now be obtained from eq.(4), to within the same approximations that were discussed in the section II A, as,

$$\mathbf{u}_\perp(\mathbf{r}) = - \sum_{j=-n/2}^{n/2} \mathbf{T}(\mathbf{r} - \mathbf{r}_j) \cdot \mathbf{F}_j^h = \frac{4\pi\eta_0 D^2}{\ln\{L/D\}} \sum_{j=-n/2}^{n/2} \mathbf{T}(\mathbf{r} - \mathbf{r}_j) \cdot (\boldsymbol{\Omega}_\perp \times \mathbf{j} \hat{\mathbf{u}}). \quad (60)$$

Replacing the sum over beads by a line integral, we thus find,

$$\mathbf{u}_\perp(\mathbf{r}) = \frac{4\pi\eta_0}{\ln\{L/D\}} \int_{-L/2}^{L/2} dl \mathbf{T}(\mathbf{r} - \mathbf{r}_p - l \hat{\mathbf{u}}) \cdot (\boldsymbol{\Omega}_\perp \times \mathbf{l} \hat{\mathbf{u}}), \quad (61)$$

where \mathbf{r}_p is the position coordinate of the rod.

Next consider a rod rotating with an angular velocity $\boldsymbol{\Omega}_\parallel$. For this case we have to resort to Faxén's theorem for rotational motion of a bead, which reads,

$$\boldsymbol{\Omega}_\parallel = - \frac{\mathbf{1}}{\pi\eta_0 \mathbf{D}^3} \mathbf{T}_j^h + \frac{\mathbf{1}}{2} \nabla_j \times \mathbf{u}_0(\mathbf{r}_j), \quad (62)$$

where, as in the translational Faxén's theorem (7), \mathbf{u}_0 is the fluid flow velocity that would have existed in the absence of bead j . The first term on the right hand-side is just Stokes rotational friction of a single bead in an unbounded fluid, while the second term accounts for hydrodynamic interaction between the beads. The important thing to note here is that the fluid flow generated by a single rotating bead is now equal to,

$$\mathbf{u}_j(\mathbf{r}) = \left(\frac{D/2}{|\mathbf{r} - \mathbf{r}_j|} \right)^3 \boldsymbol{\Omega}_\parallel \times (\mathbf{r} - \mathbf{r}_j), \quad (63)$$

so that this fluid flow is $\mathbf{0}$ along the entire center line of the rod. This implies that hydrodynamic interaction between the beads is unimportant for this case. For a long and thin rod rotating along its center line, each bead experiences a rotational friction that is practically equal to the Stokes friction, as if each bead were alone in an unbounded fluid. As a result, the total torque on the rod is simply the sum of the Stokesian torques on the beads, so that it follows immediately from Faxén's theorem (62) that,

$$\boldsymbol{\Omega}_\parallel = - \frac{\mathbf{1}}{\pi\eta_0 \mathbf{D}^2 \mathbf{L}} \mathbf{T}_\parallel^h. \quad (64)$$

Furthermore, the total fluid flow \mathbf{u}_\parallel is simply the sum of the fluid flows (63) generated by the rotating beads as if they were alone in an unbounded fluid, since hydrodynamic interaction between the beads is unimportant in the present case. Replacing the sum by a line integral thus yields,

$$\mathbf{u}_\parallel(\mathbf{r}) = \frac{D^2}{8} \int_{-L/2}^{L/2} dl \frac{\mathbf{1}}{|\mathbf{r} - \mathbf{r}_p - l \hat{\mathbf{u}}|^3} (\boldsymbol{\Omega}_\parallel \times (\mathbf{r} - \mathbf{r}_p)). \quad (65)$$

The fluid flow $\mathbf{u} = \mathbf{u}_\perp + \mathbf{u}_\parallel$ generated by a rotating rod with an arbitrary angular velocity $\boldsymbol{\Omega} = \boldsymbol{\Omega}_\perp + \boldsymbol{\Omega}_\parallel$ follows by combining eqs.(51,52) and (60,65),

$$\mathbf{u}(\mathbf{r}) = \frac{4\pi\eta_0}{\ln\{L/D\}} \int_{-L/2}^{L/2} dl \mathbf{T}(\mathbf{r} - l \hat{\mathbf{u}}) \cdot (\boldsymbol{\Omega} \times \mathbf{l} \hat{\mathbf{u}}) + \frac{\mathbf{D}^2}{8} \int_{-L/2}^{L/2} dl \frac{\mathbf{1}}{|\mathbf{r} - \mathbf{r}_p - l \hat{\mathbf{u}}|^3} ((\hat{\mathbf{u}} \cdot \boldsymbol{\Omega}) \times (\mathbf{r} - \mathbf{r}_p)). \quad (66)$$

This approximate expression will be used in the following paragraph to obtain an expression for the mobility matrices $\mathbf{M}_{ij}^{\text{TR}}$, $j = 1, 2$.

Calculation of \mathbf{M}^{TR}

In order to calculate the velocity \mathbf{v}_2 that rod 2 acquires in the flow field (66) generated by a rotating rod 1, we apply, without further discussion, the same "mean-field" approach as in the previous section. The velocity \mathbf{v}_2 is approximated by taking the fluid flow field generated by the rotating rod as a constant, equal to the average of the actual field over the center line of the rod. Hence,

$$\mathbf{v}_2 = \bar{\mathbf{u}} - \frac{\ln\{L/D\}}{4\pi\eta_0 L} \left[\hat{\mathbf{i}} + \hat{\mathbf{u}}_2 \hat{\mathbf{u}}_2 \right] \cdot \mathbf{F}_2^h, \quad (67)$$

where the average flow field in terms of the torque on rod 1 follows from eqs.(66) and (59,64), with $\boldsymbol{\Omega} = \boldsymbol{\Omega}_1$, the angular velocity of rod 1 and \mathbf{T}_1^h the torque on rod 1,

$$\begin{aligned} \bar{\mathbf{u}} &= \frac{12}{L^4} \int_{-L/2}^{L/2} dl_1 \int_{-L/2}^{L/2} dl_2 \mathbf{T}(\mathbf{r}_{21} + l_2 \hat{\mathbf{u}}_2 - l_1 \hat{\mathbf{u}}_1) \cdot (l_1 \hat{\mathbf{u}}_1 \times \mathbf{T}_1^h) \\ &+ \frac{1}{8\pi\eta_0 L^2} \int_{-L/2}^{L/2} dl_1 \int_{-L/2}^{L/2} dl_2 \frac{1}{|\mathbf{r}_{21} + l_2 \hat{\mathbf{u}}_2 - l_1 \hat{\mathbf{u}}_1|^3} (\mathbf{r}_{21} + l_2 \hat{\mathbf{u}}_2) \times (\hat{\mathbf{u}}_1 \hat{\mathbf{u}}_1 \cdot \mathbf{T}_1^h) . \end{aligned} \quad (68)$$

By definition the following ‘‘mean-field’’ expression for the translational-rotational mobility matrices are thus obtained (after an interchange of the indices 1 and 2),³

$$\mathbf{M}_{11}^{\text{TR}} = \mathbf{0} , \quad (69)$$

$$\begin{aligned} \mathbf{M}_{12}^{\text{TR}} &= \frac{12}{L^4} \int_{-L/2}^{L/2} dl_1 \int_{-L/2}^{L/2} dl_2 l_2 \hat{\mathbf{u}}_2 \times \mathbf{T}(\mathbf{r}_{12} + l_1 \hat{\mathbf{u}}_1 - l_2 \hat{\mathbf{u}}_2) \\ &+ \frac{1}{8\pi\eta_0 L^2} \int_{-L/2}^{L/2} dl_1 \int_{-L/2}^{L/2} dl_2 \frac{1}{|\mathbf{r}_{12} + l_1 \hat{\mathbf{u}}_1 - l_2 \hat{\mathbf{u}}_2|^3} [\hat{\mathbf{u}}_2 \times (\mathbf{r}_{12} + l_1 \hat{\mathbf{u}}_1)] \hat{\mathbf{u}}_2 . \end{aligned} \quad (70)$$

A non-zero contribution to $\mathbf{M}_{11}^{\text{TR}}$ stems entirely from reflection contributions, since a pure rotation of a single rod in an unbounded fluid does not induce a translational velocity of the same rod. As mentioned before, reflection contributions are small in the isotropic state, since the typical distance between the beads of different rods is of the order L .

APPENDIX B

As a first step in the evaluation of the integrals in eq.(43) for f_1 , the Fourier transform of the Oseen tensor ($\mathbf{T}(\mathbf{k}) = \frac{1}{\eta_0 \mathbf{k}^2} [\hat{\mathbf{I}} - \hat{\mathbf{k}}\hat{\mathbf{k}}]$, with $\hat{\mathbf{k}} = \mathbf{k}/k$) is substituted, and the integrations with respect to l_1 and l_2 are performed, with the result,

$$\begin{aligned} f_1 &= -\frac{1}{8\pi^5 DL} \int d\mathbf{k} k^{-2} \oint d\hat{\mathbf{u}}_1 \oint d\hat{\mathbf{u}}_2 \int d\mathbf{r}_{12} [g(\mathbf{r}_{12}, \hat{\mathbf{u}}_1, \hat{\mathbf{u}}_2) - \chi_f(\mathbf{r}_1 | \mathbf{r}_2, \hat{\mathbf{u}}_2)] \\ &\quad \times \exp\{i\mathbf{k} \cdot \mathbf{r}_{12}\} j_0\left(\frac{1}{2}L\mathbf{k} \cdot \hat{\mathbf{u}}_1\right) j_0\left(\frac{1}{2}L\mathbf{k} \cdot \hat{\mathbf{u}}_2\right) , \end{aligned} \quad (71)$$

where,

$$j_0(x) \equiv \frac{\sin\{x\}}{x} . \quad (72)$$

Consider the integral with respect to \mathbf{r}_{12} ,

$$I \equiv \int d\mathbf{r}_{12} [g(\mathbf{r}_{12}, \hat{\mathbf{u}}_1, \hat{\mathbf{u}}_2) - \chi_f(\mathbf{r}_1 | \mathbf{r}_2, \hat{\mathbf{u}}_2)] \exp\{i\mathbf{k} \cdot \mathbf{r}_{12}\} . \quad (73)$$

Replace the expression in the square brackets by $(g - 1) + (1 - \chi_f)$. The integral over $1 - \chi_f$ is easily found to be equal to,

$$\int d\mathbf{r}_{12} [1 - \chi_f(\mathbf{r}_1 | \mathbf{r}_2, \hat{\mathbf{u}}_2)] \exp\{i\mathbf{k} \cdot \mathbf{r}_{12}\} = \frac{\pi}{4} \mathbf{D}^2 L j_0\left(\frac{1}{2}L\mathbf{k} \cdot \hat{\mathbf{u}}_2\right) , \quad (74)$$

while the integral over $g - 1$ is equal to,

³ The outer product $\mathbf{a} \times \mathbf{A}$ of a vector \mathbf{a} and a matrix \mathbf{A} is defined as the matrix with column vectors equal to the outer product of \mathbf{a} and the column vectors of \mathbf{A} . The outer product is thus taken with respect to the first index on \mathbf{A} .

$$\int d\mathbf{r}_{12} [g(\mathbf{r}_{12}, \hat{\mathbf{u}}_1, \hat{\mathbf{u}}_2) - 1] \exp\{i\mathbf{k} \cdot \mathbf{r}_{12}\} = -2\mathbf{D}\mathbf{L}^2 |\hat{\mathbf{u}}_1 \times \hat{\mathbf{u}}_2| j_0(\frac{1}{2}\mathbf{Lk} \cdot \hat{\mathbf{u}}_1) j_0(\frac{1}{2}\mathbf{Lk} \cdot \hat{\mathbf{u}}_2). \quad (75)$$

These results are valid for $kD \ll 1$ (say $kD < 0.2$), while, in addition, eq.(75) is valid for orientations where $\frac{D}{L} \ll |\hat{\mathbf{u}}_1 \times \hat{\mathbf{u}}_2|$. As will turn out, the kD -dependence is of no importance for long and thin rods, since convergence of the wavevector integral is assured by the kL -dependent functions, which tend to zero for wavevectors for which, indeed, $kD \ll 1$. Moreover, the angular integration range, pertaining to orientations where $\frac{D}{L} / |\hat{\mathbf{u}}_1 \times \hat{\mathbf{u}}_2|$ is not small, vanishes for long and thin rods. Substitution of the results (74,75) into eq.(71) for f_1 , and noting that after integration over orientations the dependence on the direction $\hat{\mathbf{k}}$ of the wavevector is lost, so that its direction may be chosen along the z -direction, yields (with $x = \frac{1}{2}kL$),

$$f_1 = \frac{2}{\pi^4} \int_0^\infty dx \oint d\hat{\mathbf{u}}_1 \oint d\hat{\mathbf{u}}_2 j_0^2(x z_2) \left[|\hat{\mathbf{u}}_1 \times \hat{\mathbf{u}}_2| j_0^2(x z_1) - \frac{\pi D}{8 L} j_0(x z_1) \right]. \quad (76)$$

with z_j , $j = 1, 2$, is the z -component of $\hat{\mathbf{u}}_j$. The second term between the square brackets is an $\mathcal{O}(D/L)$ contribution as compared to the first term and may be neglected. Transforming the orientational integrals to spherical coordinates, for which $z_j = \cos\{\Theta_j\}$, and using that (with $\Psi = \varphi_1 - \varphi_2$),

$$|\hat{\mathbf{u}}_1 \times \hat{\mathbf{u}}_2| = \left[1 - (\cos\{\Theta_1\} \cos\{\Theta_2\} + \sin\{\Theta_1\} \sin\{\Theta_2\} \cos\{\Psi\})^2 \right]^{1/2}, \quad (77)$$

finally yields eq.(46) for f_1 .

Next consider the evaluation of the integrals in eq.(44) for f_2 . That the integrals are convergent follows from the Taylor expansion,

$$\frac{1}{|\mathbf{r}_{12} - \mathbf{a}|} = \frac{1}{r_{12}} + \mathbf{a} \cdot \nabla \frac{1}{r_{12}} + \frac{1}{2} \mathbf{a} \mathbf{a} : \nabla \nabla \frac{1}{r_{12}} + \dots \quad (78)$$

Using this in eq.(44) and integration with respect to $\hat{\mathbf{u}}_1$ shows that the integrand varies like $\sim r_{12}^{-4}$ for large r_{12} , since $\nabla^2 r_{12}^{-1} = 0$ for $r_{12} \neq 0$. Following the same procedure as above one finds,

$$f_2 = \frac{1}{2\pi^3 DL} \int d\mathbf{k} \int_{-1}^1 dz_1 \int_{-1}^1 dz_2 \left[(2\pi)^3 \delta(\mathbf{k}) - \frac{\pi}{4} \mathbf{D}^2 \mathbf{L} j_0(\frac{1}{2}\mathbf{Lk} z_2) \right] \times j_0(\frac{1}{2}Lk z_2) \frac{j_0(\frac{1}{2}Lk z_1) - 1}{k^2}, \quad (79)$$

where δ is the delta distribution. The second term in the square brackets is easily seen to be $\mathcal{O}(D/L)$, using the same integration tricks as above for the evaluation of f_1 . For the evaluation of the delta distribution contribution, the integrand can be expanded in a power series expansion in k . Using that $j_0(x) = 1 - x^2/6 + \dots$, results in eq.(47) for f_2 .

APPENDIX C

An analytical centrifuge measures the concentration of sedimenting colloid along the centrifugal field. From a single run in an analytical ultracentrifuge we obtain a time sequence of plots usually taken every few minutes. A representative sequence of these plots is shown in Fig. 5. Each plot in the series indicates the fd concentration as a function of radial position in the cell at that particular time. The concentrations of the dilute virus solutions were determined with the extinction coefficients of $3.84 \text{ mg}^{-1} \text{ cm}^2$ at 270 nm [7]. For samples with higher concentration the solution is optically opaque at 270 nm and therefore we measure absorbance at progressively higher wavelengths, which corresponds to a lower extinction coefficient of fd . The sedimenting particles in Fig. 5 move from left to right. The water-air interface is indicated by a sharp peak located at radial position of 5.95 cm that is due to refraction by the meniscus. Note that this peak does not move as a function of time indicating that the container does not leak. As the rods start sedimenting towards the cell bottom, the region at the top of the solution (to the right of the air-water interface and to the left of the sedimentation front in Fig. 5) is depleted of virus as indicated by absence of absorbance. Also the value of the concentration of rods in the plateau region, always to the right of the depleted region, is decreasing as the bulk of the sample moves towards the bottom of the container. The reason for this is that the walls of the cell are not parallel to each other, but instead follow the lines of centrifugal field in order to

minimize convective disturbances, an effect referred to as “radial dilution” [15]. Between the flat plateau region and the depleted region there is a sharp boundary.

At higher concentrations of fd we observed the appearance of a sharp peak at the sedimenting boundary as is shown in Fig. 6. The peak height increases with increasing concentration while the magnitude of the peak is independent of the wavelength and thus this peak cannot be due to absorption of the fd , which is wavelength dependent. The probable cause of the peak is the refraction of incident light due to the steep gradient in the virus concentration and hence the refractive index at the sedimenting boundary. As the incident light is refracted away from the detector, less light is collected by it and this results in apparent increased absorption of the sample. The peak at the water/air meniscus has the same origin.

Two factors that determine the shape of the sedimenting boundary are the diffusion constant and the self-sharpening effect [17]. The diffusion of the particles leads to gradual spreading of the initially very sharp boundary. This diffusion of particles is countered by the self-sharpening effect, which is due to the concentration dependence of the sedimentation velocity. On one hand, any molecule lagging behind the boundary is in a more dilute environment and will therefore sediment at an enhanced velocity. On the other hand, the particles in the plateau region are in a more concentrated environment and their sedimentation will be retarded. As a consequence the boundaries will self-sharpen. In a suspension of elongated particles the self-sharpening effect will be much stronger than in a suspension of globular particles because the volume prefactor α in Eq. 49 is much larger for elongated particles than for globular particles. The pronounced self-sharpening effect leads to hyper-sharp boundaries, which result in a steep gradient of refractive index which in turn causes the artifacts shown in Fig. 6. In globular colloids these effects are usually not observed.

In sedimentation analysis it is assumed that the rate of movement of the sedimentation boundary is approximately equivalent to the sedimentation velocity of the particles in the plateau (bulk) region. To compare results from different runs it is usual to express the sedimentation velocity in units independent of centrifugal force as follows:

$$S = \frac{1}{\omega^2 r} \frac{dr}{dt} = \frac{1}{\omega^2} \frac{d \ln r}{dt} \quad (80)$$

The sedimentation velocity unit is called a Svedberg (S), with $1 \text{ S} = [10^{-13} \text{sec}^{-1}]$. We define r as the radial position at the sedimentation boundary where the virus concentration is equal to half the concentration of the plateau region. This quantity is easily obtained from experimental data for samples at low concentration. For samples at higher concentration, where we observe a peak at the sedimenting boundary due to refraction of light, we define r as the radial position of the highest point of the peak. A typical plot of the logarithm of r against $\omega^2 t$ used in the determination of the sedimentation constant is shown in Fig. 7. Surprisingly, we found out that a linear function provided an inadequate fit to our data. When the sedimentation data are collected between radial positions of 6.1 cm and 6.8 cm a polynomial of second order fits the data much better:

$$\ln r = A + B\omega^2 t + C\omega^4 t^2 \quad (81)$$

We introduce the experimentally observed sedimentation constant S^r by combining Eq. 81 and Eq. 80:

$$S^r = \frac{d \ln r}{d\omega^2 t} = B + 2C\omega^2 t \quad (82)$$

From this equation we see that the experimentally measured sedimentation velocity is not a constant but depends on the position of the measurement r or equivalently time $\omega^2 t$ at which the sedimentation front is found at position r . The reason for this unexpected behavior is not clear, but we assume it is an instrumental artifact. There is no physical reason to believe that the sedimentation velocity is a function of time or of radial position in the cell. In table 1 we see that the coefficient C , obtained when the quadratic polynomial in Eq. 81 is fitted to data in Fig. 4a is independent of concentration. This is another indication that this artifact is due to the instrument.

Theoretically, the constant B in eq. (82) should be equal to the concentration dependent Svedberg constant:

$$S_\phi = S_0(1 - \alpha\phi) \quad (83)$$

and the constant C should be zero. Instead, we have found that the experimental Svedberg (eq. 82) is described by:

$$S^r = S_\phi + \text{offset} = S_0 + \text{offset} - S_0\alpha\phi \quad (84)$$

where “offset” depends on position in the centrifuge, but is independent of colloid concentration. S_0 is the Svedberg constant of the rods in the limit of zero concentration. However, the value of slope

$$\frac{dS^r}{d\phi} = \alpha S_0 \tag{85}$$

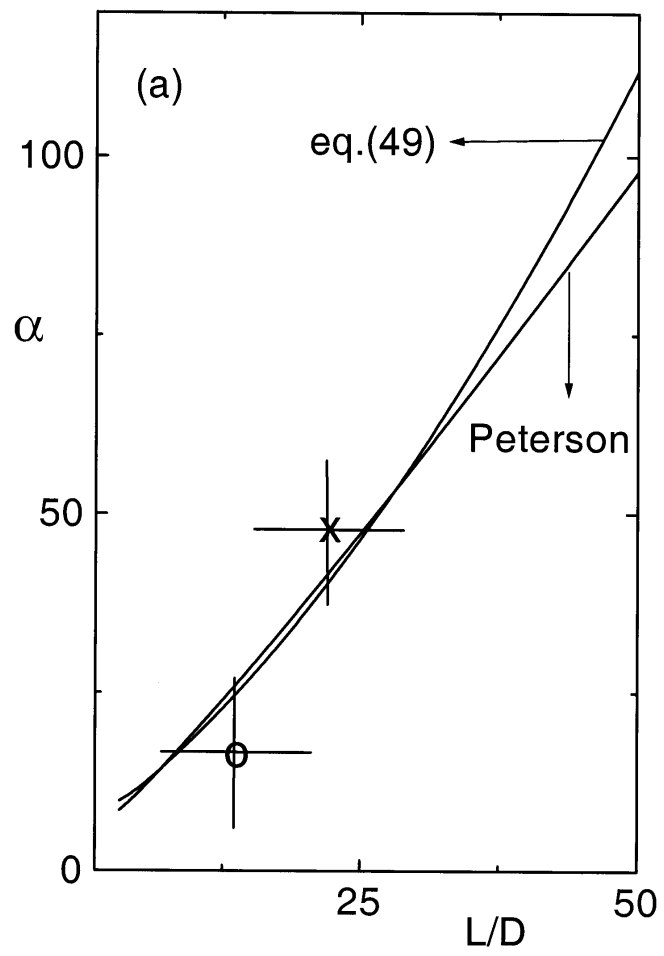
is independent of radial position (or equivalently $\omega^2 t$) where we evaluate Eq. 82 as is shown in table I. The measurement artifact only introduces a position dependent offset in the sedimentation velocity which affects the measured value of S_0 . From a few measurements where we did not observe measurement artifacts ($C = 0$) we obtained the value of $S_0 = 47$. Since this is in good agreement with previous measurements we use this value throughout our analysis [18].

It is important to note that the dependence of S^r on position r shown in Fig. 7 is not due to the decreasing concentration of rods in plateau, which in turn is due to radial dilution. To show this we have made two measurements. In a first measurement we evaluated the sedimentation velocity at the point where the sedimenting boundary is close to the bottom of the container. At this time, due to radial dilution, the plateau concentration is about 70% of the initial concentration. In the second run our initial concentration was 70% of the concentration of rods in the first run. In this run we evaluated the sedimentation velocity right at the beginning of the run. We find that sedimentation velocities obtained in these two ways are vastly different, which indicates that the systematic errors described are not due to radial dilution.

References

★ Author to whom the correspondence should be addressed

1. A.P. Philipse, *Current Opinion in Coll. and Int. Sci.* **2**, 200 (1997).
2. G.K. Batchelor, *J. Fluid Mech.* **52** 245 (1972).
3. J. M. Peterson, *J. Chem. Phys.* **40** (1964) 2680.
4. J. García de la Torre, V.A. Bloomfield, *Quarterly Reviews of Biophysics* **14**, 81 (1981).
5. D. M. E. Thies-Weesie, *Sedimentation and liquid permeation of inorganic colloids*, PhD thesis, Universiteit Utrecht, 1995
6. S. Fraden, in *Observation, Prediction, and Simulation of Phase Transitions in Complex Fluids*, edited by M. Baus, L. F. Rull and J. P. Ryckaert (Kluwer, Dordrecht, 1995)
7. S. A. Berkowitz and L. A. Day, *J. Mol. Biol.* **102**, 531, (1976).
8. L. Song, U. Kim, J. Wilcoxon and J. M. Schurr, *Biopolymers*, **31**, 547 (1991).
9. K. Zimmermann, H. Hagedorn, C. C. Heuck, M. Hinrichsen and H. Ludwig, *J. Biol. Chem.*, **261**, 1653 (1986)
10. J. Sambrook, E. F. Fritsch and T. Maniatis, *Molecular Cloning: a laboratory manual*, (Cold Spring Harbor Laboratory Press, New York, 1989).
11. R. Buscall, J. W. Goodwin, R. H. Ottewill and Th. F. Tadros, *J. Colloid Interface Sci.*, **85**, 78 (1982).
12. D. M. E. Thies-Weesie, A. P. Philipse, G. Nagele, B. Mandl and R. Klein, *J. Colloid Interface Sci.*, **176**, 43 (1995).
13. J. K. G. Dhont, *An Introduction to Dynamics of Colloids*, (Elsevier Science, Amsterdam, 1996).
14. L. Onsager, *Ann. N. Y. Acad. Sci.* **51**, 627 (1949).
15. J. Tang and S. Fraden, *Liquid Crystals* **19**, 459 (1995).
16. M. Doi and S. F. Edwards, *The Theory of Polymer Dynamics*, (Clarendon Press, Oxford, 1986)
17. E. Schachman, *Ultracentrifugation in Biochemistry*, (Academic Press, New York, 1959).
18. J. Newman, H. L. Swinney, and L. A. Day, *J. Mol. Biol.* **116**, 593, 1977



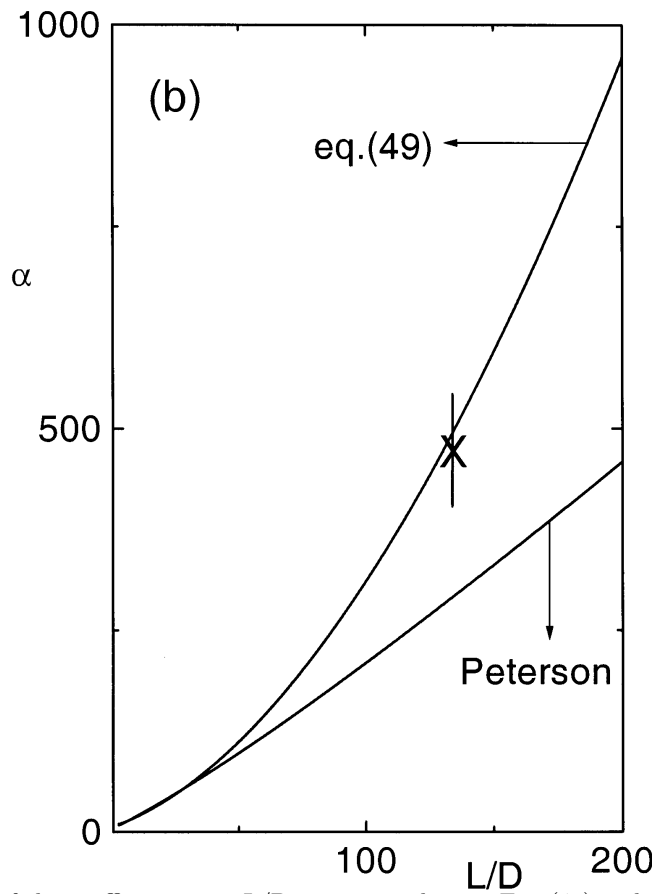


FIG. 1. a) The dependence of the coefficient α on L/D ratio according to Eq. (49) and to Peterson [3]. The coefficient α is the first order correction to sedimentation velocity due to finite concentration of the colloidal rods. The two data points are for silica rods. b) The coefficient α for $L/D < 200$. The data point is for *fd*-virus, as obtained in the experimental section of the present paper

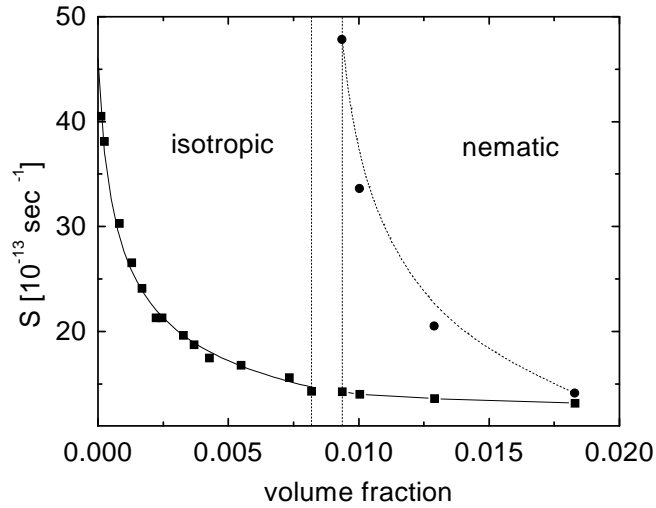


FIG. 2. Dependence of sedimentation velocity of rods measured in Svedberg's (Eq. 82) on the average volume fraction of fd at an ionic strength of 8 mM, pH 8.2. The equation of the fitted curve is $S(\phi) = 46.0(1 + 3600\phi)^{-1/3}$. A sample made with a volume fraction between the two dashed vertical lines is unstable and will spontaneously phase separate into an isotropic phase at volume fraction of 0.0081 and a nematic phase at volume fraction 0.0093. When rods are sedimented in the nematic phase of initial volume fraction as indicated in the nematic region of the plot, we observe two sedimenting boundaries with two different velocities and two different concentrations. The sedimentation velocity of the faster moving component is indicated with filled circles, while the sedimentation velocity of slower moving boundary is indicated with filled squares. The actual volume fraction of the slower moving component is approximately constant at 0.0081 implying that that component is in the isotropic phase. The concentration of the faster component increases with the average concentration and is always concentrated enough to be a nematic phase.

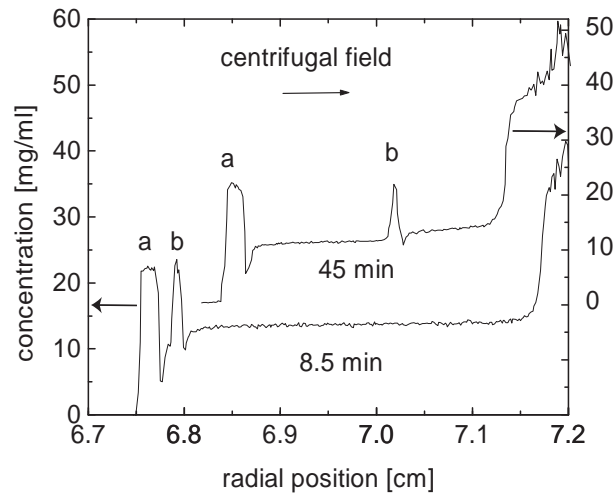


FIG. 3. A concentration profile of sedimenting *fd* virus in a nematic(cholesteric) phase taken at two different times. Instead of a single moving boundary and a single plateau we observe two moving boundaries and two plateaus. Increased absorbance at the bottom of the container is due to the accumulation of the virus particles. Peak “b” marks the fast sedimenting nematic boundary while peak “a” marks the slow sedimenting isotropic boundary. The two curves are offset for clarity. The concentration of the initially uniform nematic sample was 13 mg/ml. The concentration of the co-existing isotropic and nematic phases at 8 mM ionic strength is 10.5 mg/ml and 12 mg/ml, respectively.

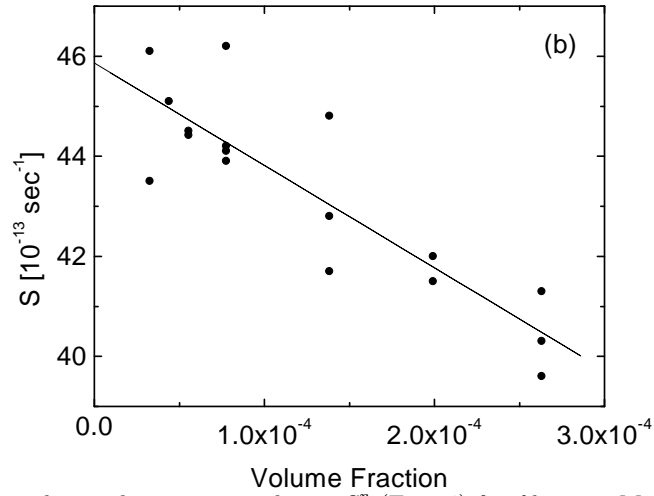
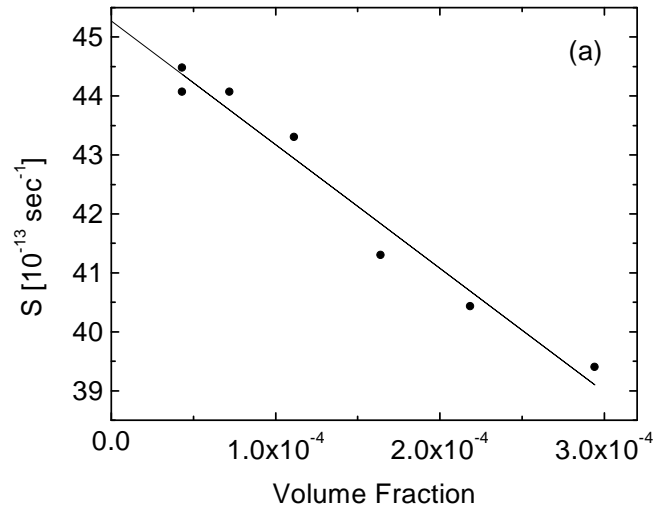


FIG. 4. a) Concentration dependent sedimentation velocity S^r (Eq. 84) for fd at 50mM ionic strength. The data is fitted to a linear function $S^r = 45.3 - 20980\phi$. The solid line is given by Eq. 85, which yields αS_0 . The overlap volume fraction for fd with $L=880$ nm is $5.9 \cdot 10^{-5}$. b) Concentration dependent sedimentation velocity for fd at 100mM ionic strength. The data is fitted to a linear function $S^r = 45.9 - 20450\phi$.

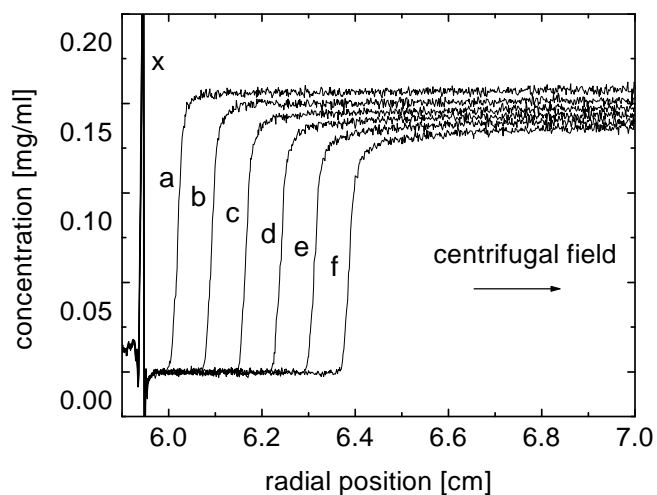


FIG. 5. Data obtained from an analytical centrifuge. A time series of the fd concentration as a function of radial position in the centrifuge taken at 6.5 min intervals with “a” the first scan and “f” the last. The steep step in concentration represents the sedimentation front, which moves away from the centrifuge rotation axis with time. In this particular case the centrifuge was spun at 25000 rpm and the centrifugal (sedimenting) field points from left to right. The sharp peak “x” at the radial position of 5.95 cm is due to refraction by the air-water meniscus. Radial dilution accounts for the diminishing plateau concentration with increasing time.

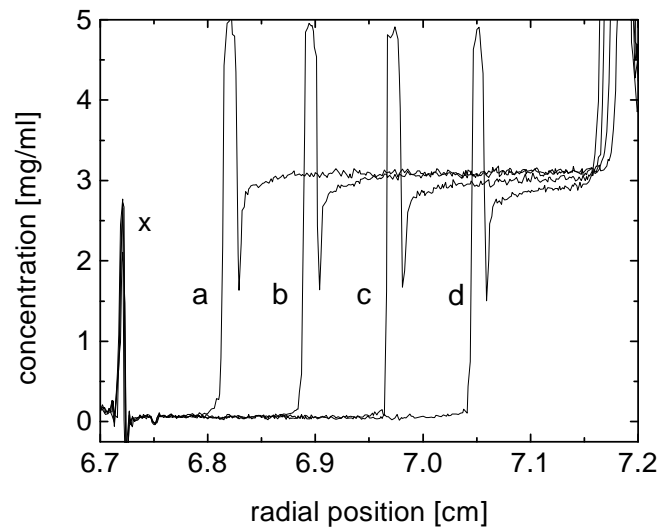


FIG. 6. A series of plots of fd concentration as a function of radial position at time intervals of approximately 12.7 min with “a” the first scan and “d” the last. The difference between this series and those in Fig. 5 is that here the concentration of fd is higher and the rotation speed was 20,000 rpm. The peak seen at the sedimenting boundary is an artifact of the detection system and is due to the refraction of light at a sharp step in the refractive index at the sedimenting boundary. Radial dilution lowers the plateau concentration with time. A similar peak occurs at the air/water meniscus “x”, which is stationary.

Volume fraction	$S^{6.1\text{cm}}/10^{-13}\text{s}^{-1}$	C	$S^{6.8\text{cm}}/10^{-13}\text{s}^{-1}$
$4.31\cdot 10^{-5}$	44.1	$1.35\cdot 10^{-23}$	49.5
$4.31\cdot 10^{-5}$	44.5	$1.27\cdot 10^{-23}$	49.6
$7.21\cdot 10^{-5}$	44.1	$1.21\cdot 10^{-23}$	48.9
$1.11\cdot 10^{-4}$	43.3	$1.26\cdot 10^{-23}$	48.3
$1.64\cdot 10^{-4}$	41.3	$1.17\cdot 10^{-23}$	45.9
$2.18\cdot 10^{-4}$	40.4	$1.27\cdot 10^{-23}$	45.5
$2.94\cdot 10^{-4}$	39.4	$1.35\cdot 10^{-23}$	44.8

TABLE I. The values of constants obtained from Eq. 82 being fitted to data from Fig. 4a. The second column indicates the value of the sedimentation velocity S^r evaluated at the start of the sedimentation experiment at $\omega^2 t = 0$ or equivalently $r=6.1\text{cm}$. The third column indicates the value of parameter C in Eq. 82, which is independent of concentration. If we evaluate Eq. 82 for the sedimentation velocity at the end of the sedimentation experiment $r=6.8\text{ cm}$, we obtain the values of the sedimentation velocity shown in the fourth column. Note that the value of the slope αS_0 (Eq. 84) does not depend on the radial position. The value of αS_0 from the data evaluated at $r=6.1\text{cm}$ is 20,500 and at $r=6.8\text{ cm}$ is 21,000. We use the value $S_0 = 47$ to obtain α .

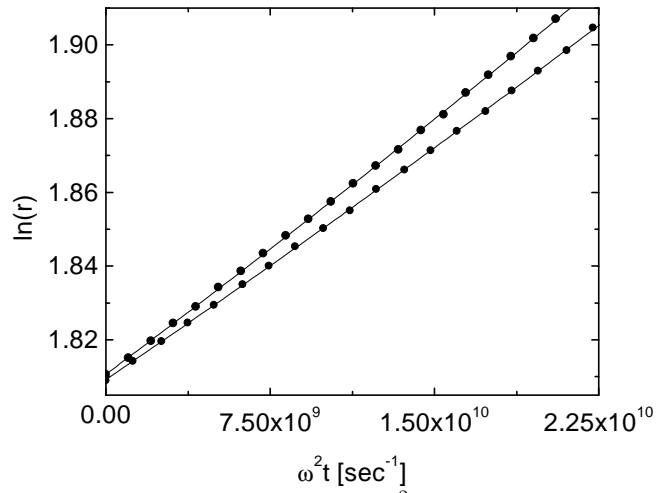


FIG. 7. Position of the sedimentation boundary plotted against $\omega^2 t$. The circles represent measurements which were taken approximately every 2.5 min. The lines represent the second order polynomial fit to the data (Eq. 81). The plot with a larger slope corresponds to the sedimentation of *fd* virus in 100mM ionic strength at a volume fraction of $7.75 \cdot 10^{-5}$ at 25,000 rpm. The other plot is for a higher volume fraction of *fd* equal to $2.63 \cdot 10^{-4}$.